

PanBench: Towards High-Resolution and High-Performance Pansharpening

Shiying Wang^{1,*}, Xuechao Zou^{1,*}, Kai Li², Junliang Xing², Pin Tao^{1,2,†}

¹Department of Computer Technology and Applications, Qinghai University, Xining, China

²Department of Computer Science and Technology, Tsinghua University, Beijing, China

wangshiying.qhu@foxmail.com, xuechaozou@foxmail.com, tsinghua.kaili@gmail.com,

jlxing@tsinghua.edu.cn, taopin@tsinghua.edu.cn

Abstract

Pansharpening, a pivotal task in remote sensing, involves integrating low-resolution multispectral images with high-resolution panchromatic images to synthesize an image that is both high-resolution and retains multispectral information. These pansharpened images enhance precision in land cover classification, change detection, and environmental monitoring within remote sensing data analysis. While deep learning techniques have shown significant success in pansharpening, existing methods often face limitations in their evaluation, focusing on restricted satellite data sources, single scene types, and low-resolution images. This paper addresses this gap by introducing PanBench, a high-resolution multi-scene dataset containing all mainstream satellites and comprising 5,898 pairs of samples. Each pair includes a four-channel (RGB + near-infrared) multispectral image of 256×256 pixels and a mono-channel panchromatic image of $1,024 \times 1,024$ pixels. To achieve high-fidelity synthesis, we propose a Cascaded Multiscale Fusion Network (CMFNet) for Pansharpening. Extensive experiments validate the effectiveness of CMFNet. We have released the dataset, source code, and pre-trained models in the supplementary, fostering further research in remote sensing.

1. Introduction

With the continuous advancement of remote sensing technology, a substantial amount of earth observation data can be readily obtained. Due to the technological constraints of remote sensing imaging sensors, remote sensing images are typically provided as low-resolution multispectral (MS) images and high-resolution panchromatic (PAN) images. The task of pansharpening [48] has emerged to obtain images with high spatial and spectral resolutions. Pansharpening aims to reconstruct a high-resolution MS image from a low-resolution MS image guided by a PAN image. The pansharpened images enable better analysis and interpretation of the data, serving as an indispensable preprocessing

step for downstream tasks in remote sensing, such as land cover classification [4, 31], object recognition [22, 25], and change detection [1, 43]. It provides high-quality data for downstream remote sensing [5, 18, 42] applications.

Deep learning methods [10, 12, 32, 39] have been widely applied in recent years and have made significant progress in pansharpening. It usually utilizes deep neural network models [15, 21] to learn the complex mapping relationship between MS and PAN images through end-to-end training.

Existing deep learning-based pansharpening algorithms for remote sensing images can be broadly categorized into three types: 1) pixel-level fusion, 2) feature-level fusion, and 3) pixel-feature-level fusion. Pixel-level fusion splices the up-sampled MS image and PAN image directly on the channel dimension and then inputs them into the neural model for processing. Such as PNN [33], MSDCNN [46], GPPNN [44] and so on. While pixel-level fusion is easy to implement, it may potentially destroy the spectral information of the MS image, resulting in fused images that are not sufficiently clear in certain scenarios. Feature-level fusion is to extract modality-aware features from the panchromatic and multispectral images independently, followed by information fusion in the feature space. Algorithms in this category include PanNet [45], TFNet [29], FusionNet [9], among others. This kind of method can better retain the band information of MS images. Still, it needs many transformations and calculations and is easily affected by the feature extraction algorithm. Pixel-feature-level fusion refers to injecting PAN images as reference information into the network in stages based on image super-resolution tasks to guide the entire spatial information reconstruction process. Such as SFIIN [50], MIDP [51]. Some of these algorithms introduce an information-driven framework to reduce redundancy and enhance model performance.

Although deep learning-based pansharpening methods for remote sensing images have achieved promising results, numerous challenges and issues remain to be addressed. On the one hand, the current research on pansharpening relies on small-scale patch cropping, limited satellite sources, and

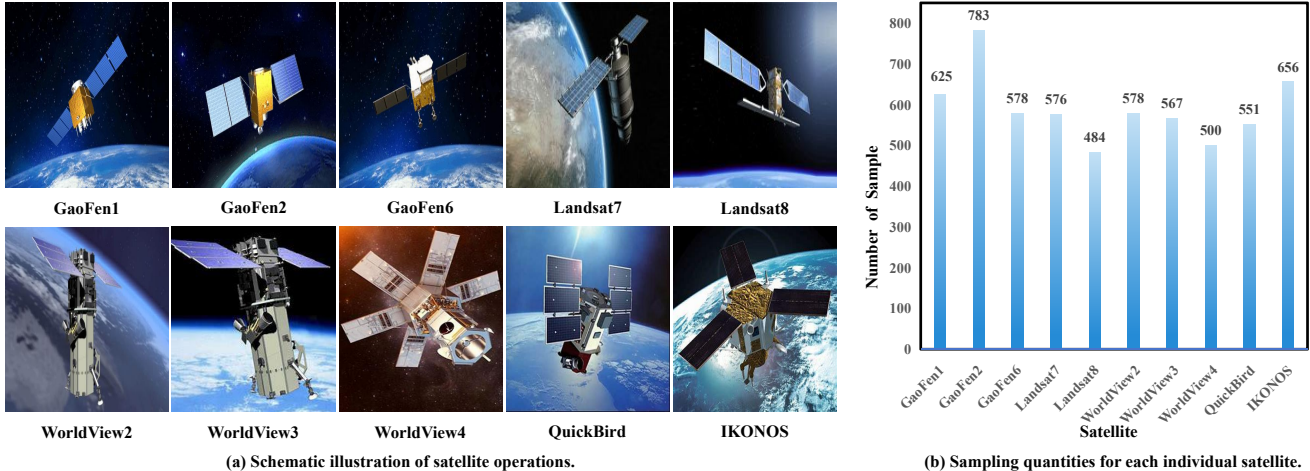


Figure 1. All mainstream satellites for pansharpening are supported by our PanBench dataset.

Table 1. Comparative analysis of the PanBench dataset against datasets used in other representative literature.

Method	Publication	Year	GF1	GF2	GF6	LC7	LC8	WV2	WV3	WV4	QB	IN	PAN
PNN [33]	Remote Sens.	2016						✓				✓	132×132
PanNet [45]	ICCV	2017						✓	✓			✓	400×400
MSDCNN [46]	J-STARS	2018						✓			✓	✓	164×164
TFNet [29]	Inform. Fusion	2020	✓								✓		512×512
FusionNet [9]	TGRS	2020		✓				✓	✓		✓		64×64
PSGAN [27]	TGRS	2020		✓				✓			✓		256×256
GPPNN [44]	CVPR	2021		✓			✓				✓		128×128
SRPPNN [3]	TGRS	2021					✓		✓		✓		256×256
MDSSC-GAN [11]	TGRS	2021							✓				512×512
MIDP [51]	CVPR	2022		✓				✓	✓				128×128
SFIIN [50]	ECCV	2022		✓				✓	✓				128×128
PanDiff [35]	TGRS	2023		✓				✓	✓		✓		64×64
USSCNet [28]	Inform. Fusion	2023						✓	✓			✓	256×256
PGCU [53]	CVPR	2023		✓				✓	✓				128×128
CMFNet [Ours]	-	2023	✓	✓	✓	✓	✓	✓	✓	✓	✓	✓	1024×1024

a single category of scenes, which can lead to poor overall generalization capability of the models. On the other hand, in the existing methods, MS and PAN are usually concatenated for channel splicing, the feature extraction process is coupled, and the cascade is not considered for multiscale fusion, which indirectly increases the difficulty of image detail recovery. Therefore, a unified high-resolution dataset and stable high-performance baseline are urgently needed for pansharpening to better meet the requirements of practical applications. We have compiled a more comprehensive dataset, PanBench, to address the issue mentioned above by gathering remote sensing data from multiple satellites. Subsequently, based on this dataset, we introduce the Cascaded Multiscale Fusion Network (CMFNet). Hierarchical image feature extraction is performed on the input PAN and MS

images, respectively, and dense cascade and top-down cascade addition are used to improve the interconnection between the features of the decoding layer. The hierarchical feature maps are directly densely connected, and all coarse low-dimensional features are exploited to generate satisfactory high-resolution depth outputs without much attenuation through the decoding layers. Thus, the fused features are decoded to restore the pansharpening image.

2. Related Work

2.1. Datasets for Pansharpening

The dataset plays a crucial role in developing and evaluating pansharpening algorithms. However, previous research (Tab. 1) exhibits issues in the following aspects: 1) The

majority of studies employ two to four satellite images to train and validate the effectiveness of pansharpening algorithms. Among them, GaoFen2 (GF2), IKONOS (IN), QuickBird (QB), WorldView2 (WV2), and WorldView3 (WV3) are commonly used. For instance, PanNet [45] utilizes IN, WV2, and WV3 datasets, while FusionNet [9] employs GF2, QB, WV2, and WV3 datasets. However, satellite data sources are relatively limited, and the algorithm’s generalization on other satellites needs to be verified. 2) The input multispectral scales are small. For example, PS-GAN [27] and RSIF [19] use 64×64 MS images as input, while MIDP [51] and SFIIN [50] adopt 32×32 MS images as input. It is not competent for batch processing tasks with large-resolution remote sensing images of the real world. 3) The datasets used did not specify land cover categories or included only a single category, such as PGCU [53], PanDiff [35], and USSCNet [28].

This paper constructs PanBench (Fig. 1), a large-scale, high-resolution, and multi-scene dataset containing all major satellites used for pansharpening. To ensure the scene’s diversity, according to [7, 8], the scene from PanBench is divided into water, urban, ice/snow, crops, vegetation, and barren. It ensures the algorithm can effectively handle different scenarios and produce reliable results.

2.2. Algorithms for Pansharpening

Pansharpening aims to fuse low-resolution MS images with high-resolution PAN images to obtain high-resolution MS images. In recent years, deep learning-based [17] pansharpening methods have received significant attention, which relies on large-scale data to learn the nonlinear relationship between ideal fused high-resolution MS images and low-resolution MS and PAN images. In general, deep learning-based pansharpening methods take the original MS as the ground truth based on Wald protocol [40], conduct network training under reduced resolution, and apply the trained model to the original PAN and MS images directly to obtain full-resolution fusion images. Typical pansharpening methods based on deep learning mainly include two kinds of network structures: single-branch and double-branch. For instance, inspired by the success of residual networks [13], Yang *et al.* [45] proposed a deep network called PanNet for pansharpening, which is trained in the high-pass domain to preserve spatial information. The up-sampled MS image is added to the output of the final network through residual connections, thereby preserving spectral information. Cai *et al.* [3] developed a novel convolutional neural network-based deep super-resolution pansharpening algorithm (SRPPNN) that uses multiscale features in MS images to reconstruct spatial information. Distinguishing the single-branch structure above, two-branch structures usually extract features from PAN and low-resolution MS images, respectively, and then fuse them in hidden space to

reconstruct high-resolution MS images. For example, Xu *et al.* [44] proposed a new paradigm combining depth expansion and observation models to develop model-driven pansharpening network GPPNN. This pansharpening model takes PAN and low-resolution MS images into account. However, the above pansharpening methods did not explicitly perform complementary learning of information between PAN and MS images, further limiting the performance. Man Zhou *et al.* [50] proposes a new mutual information-driven pansharpening framework, which can reduce information redundancy and improve model performance. Zhu *et al.* [53] has developed a new probability-based global cross-modal up-sampling method for translation sharpening, taking full advantage of the global information of each pixel in low-resolution MS images and the cross-modal information of guided PAN images. However, the existing methods do not consider the cascaded fusion of multi-scale spectral information and spatial information, resulting in unstable image synthesis performance.

3. PanBench Dataset

We construct the PanBench, a novel unified evaluation dataset for pansharpening, which supports 10 mainstream satellites, contains 5,898 high-resolution sample pairs, and has 6 manually labeled land cover classifications. This enables us to capture the challenges of complexity and variability encountered in practical generalization applications and contributes to further advancements in this field.

3.1. Multi-Source Satellite

A broader range of data sources is required to develop effective algorithms for pansharpening tasks under various conditions. The PanBench created includes the primary satellite sources currently available for pansharpening, as shown in Fig. 1 (a). Not all satellites support pansharpening, and some satellites, such as Sentinel-2, do not meet pansharpening’s conditions because it does not mount sensors that capture the panchromatic band. The commonly used pansharpening in the GaoFen series includes GF1 and GF2. PanBench adds the GF6 data set. The GF1, GF2, and GF6 datasets contain 625, 783, and 578 image pairs, respectively. The Worldview series also supplements the WV4 dataset based on the commonly used WV2 and WV3. The WV2, WV3, and WV4 datasets contain 578, 567, and 500 image pairs, respectively. The Landsat series adds the LC7 dataset (576 image pairs) to the LC8 dataset (484 image pairs). In addition, there are frequently used QB (551 image pairs) and IN (656 image pairs) datasets (Fig. 1 (b)). Thereby, the model can learn the characteristics and rules of satellites more comprehensively and accurately and improve the robustness of the model.

3.2. Pre-Processing

Loading the whole large remote sensing image may occupy a lot of computing resources and time. The data size can be reduced and the efficiency of data processing can be improved by clipping the image. Firstly, we performed a series of pre-processing operations on the collected source data: radiometric calibration [24], atmospheric correction [23], orthometric correction [2] and image alignment to initially extract and enhance useful information in the images. Secondly, we segmented the entire large-scale remote sensing image into some image pairs, which were composed of four-channel (RGB + near-infrared) MS images with a 256×256 pixel size and single-channel PAN images with a $1,024 \times 1,024$ pixel size. The clipping scale is the largest compared with the training data set in the current representative literature. The larger the image size, the more detail, context information, and pixel information can be captured, helping to accurately capture the subtle features and structure in the image. For Landsat7 and Landsat8, the spatial resolution of the MS component is half that of the PAN. In other cases, the MS component’s spatial resolution is a quarter of the PAN’s. Ultimately, PanBench comprises 5,898 image pairs.

3.3. Scene Classification

The ultimate objective of pansharpening is to use fused images to provide crucial spatial information for downstream tasks such as urban planning, land management, disaster response, and more. Therefore, it is necessary to verify the accuracy of the pansharpening method in various scenarios. In this study, by labeling the training data of different scenarios, we reclassified the data into six basic land cover types according to DeepGlobe 2018 [8] and Cheng *et al.* [7], Meng *et al.* [34]: water, urban, ice/snow, crops, vegetation, and barren. The specific sample counts are shown in Fig. 2. The algorithm’s performance in different scenes may differ, so optimizing the model’s parameters and the algorithm design is necessary by verifying and evaluating different scenes.

4. Method

4.1. Overall Framework

4.1.1 Problem Definition

The purpose of the pansharpening is to fuse a low-resolution MS image $\mathbf{x}_{ms} \in \mathbb{R}^{4 \times \frac{H}{4} \times \frac{W}{4}}$ with a high-resolution PAN image $\mathbf{x}_{pan} \in \mathbb{R}^{1 \times H \times W}$ to produce a high-resolution color image $\mathbf{y} \in \mathbb{R}^{4 \times H \times W}$ with multispectral information, where C , H and W represent the channels, height and width of the image, respectively. Pansharpening’s task flow can be expressed in the following formula:

$$\mathbf{y} = \mathbf{f}_\theta(\mathbf{x}_{ms}, \mathbf{x}_{pan}), \quad (1)$$

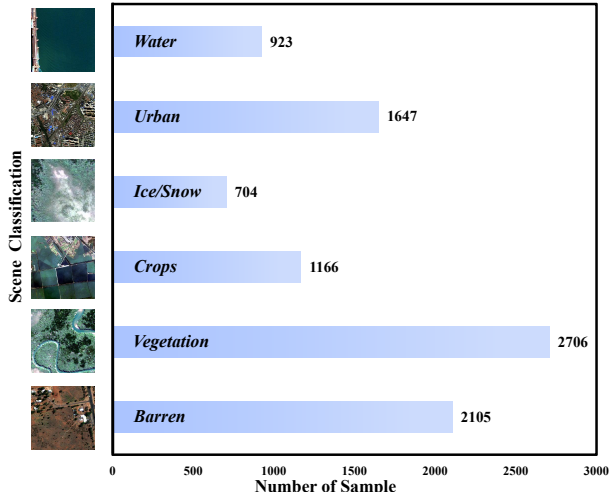


Figure 2. Number of six scenes of land cover classification.

where \mathbf{f}_θ is a parameterized neural network model.

4.1.2 Overall Pipeline

In this paper, we proposed the CMFNet, a high-fidelity fusion network for pansharpening. It primarily consists of three components: the multiscale MS encoder, the multiscale PAN encoder, and the multiscale fusion autoencoder.

The overall pipeline of the CMFNet is illustrated in Fig. 3, which is described as follows:

- **Multiscale MS Encoder.** The MS image x_{ms} passes through a convolutional layer with a kernel size of 3×3 to obtain the features $\mathbf{F}_s \in \mathbb{R}^{4C \times \frac{H}{4} \times \frac{W}{4}}$. The features are passed through a multiscale MS encoder, obtaining hierarchical image features of three resolutions.
- **Multiscale PAN Encoder.** Similar to the multiscale MS encoder, the PAN features $\mathbf{F}_p \in \mathbb{R}^{C \times H \times W}$ are pre-extracted without changing the image size, and three features corresponding to the MS scale are obtained by the multiscale PAN encoder.
- **Multiscale Fusion Autoencoder.** The fused features $\mathbf{F}_o \in \mathbb{R}^{C \times H \times W}$ are obtained from the features of the three corresponding scales obtained from the multiscale MS encoder and the PAN encoder, respectively. Finally, the fused features are output by a convolution layer.

4.2. Cascaded Multiscale Fusion Network

4.2.1 Multiscale MS Encoder

Ground objects and scenes have different characteristics at different scales due to their various sizes and shapes. Through multiscale feature extraction, the pansharpening network can focus on local details and global structure at the same time, to better capture the subtle changes and context

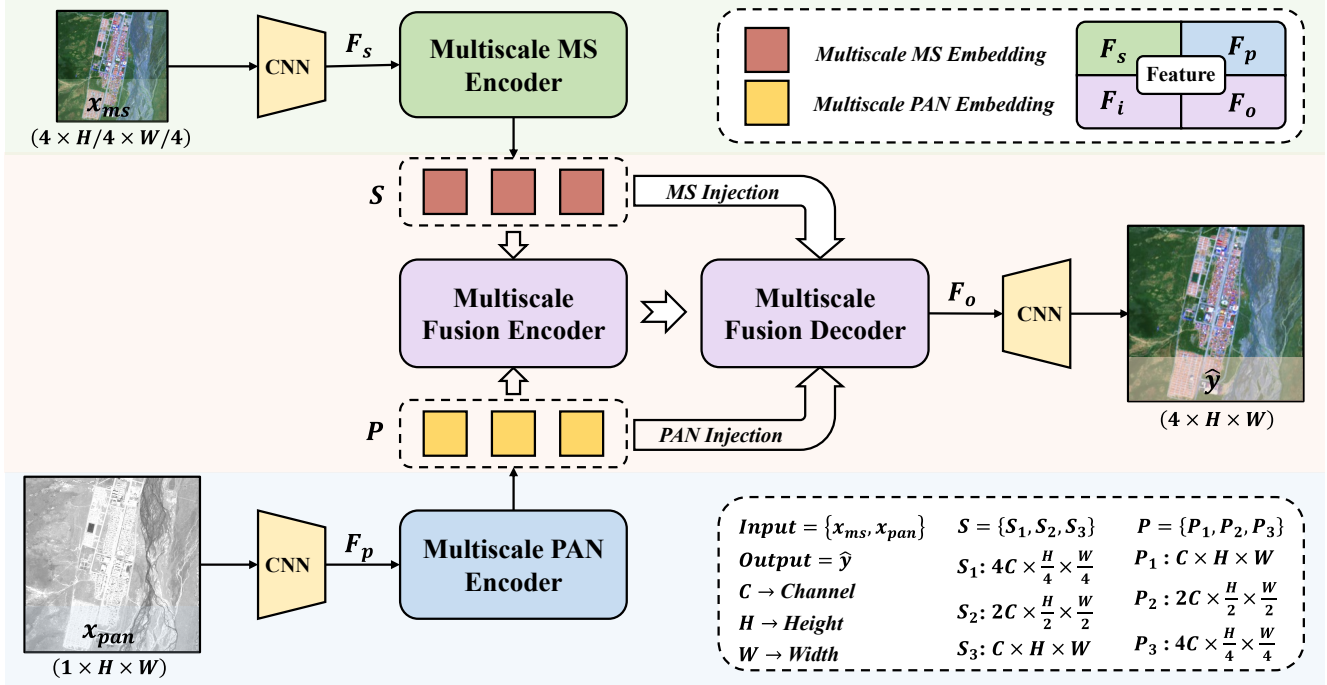


Figure 3. The overall framework of our proposed CMFNet, where F_i and F_o represent the input and output of the autoencoder, respectively.

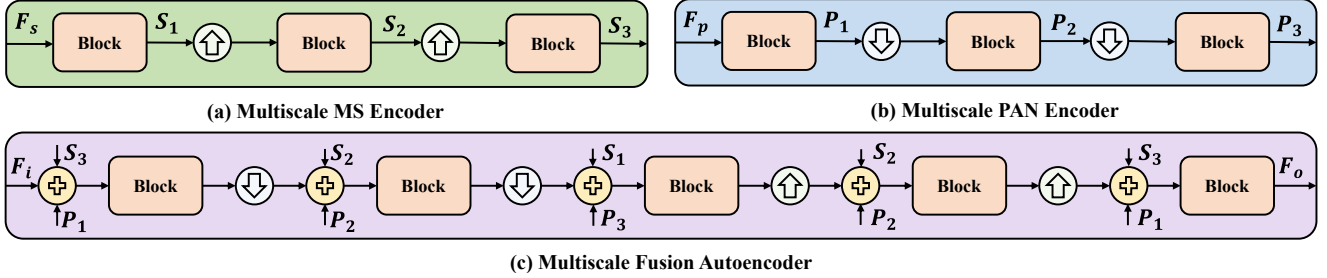


Figure 4. The detailed structure of three components in the CMFNet: (a) Multiscale MS encoder, (b) Multiscale PAN encoder, (c) Multiscale fusion autoencoder. The upward and downward arrows indicate upsampling and downsampling, respectively, while the plus sign denotes summation. The term “block” can be substituted by any module, such as ResNet [14], NAFNet [6], ConvNeXt [30] block, etc. The autoencoder integrates spectral and spatial information by incorporating identical-scale features from injecting two encoders.

information of ground objects. We introduce the multiscale MS encoder module within the CMFNet network, as shown in Fig. 4 (a). The features F_s of the MS are processed through three blocks [54] and two upsampling operations, yielding three features at distinct resolutions, denoted as $S = \{S_i \in \mathbb{R}^{(C \times 2^{3-i}) \times \frac{H}{2^{(3-i)}} \times \frac{W}{2^{(3-i)}}} \mid i \in [1, 2, 3]\}$, where the upsampling operation denotes the interpolation method.

4.2.2 Multiscale PAN Decoder

PAN images have higher spatial resolution than MS images. Multiscale feature extraction of PAN images can compensate for the lack of spatial perception of MS images and

capture a wide range of structures and spatial relationships from PAN images to better guide the pansharpening process and improve the clarity and quality of pansharpening results. Therefore, we design the multiscale PAN encoder module in the CMFNet network, as shown in Fig. 4 (b). For the PAN image feature F_p , three features corresponding to the scale of MS are obtained by three blocks, same as MS encoder and two downsampling operations, that is, $P = \{P_i \in \mathbb{R}^{(C \times 2^{i-1}) \times \frac{H}{2^{(i-1)}} \times \frac{W}{2^{(i-1)}}} \mid i \in [1, 2, 3]\}$, where the downsampling operation denotes the pooling layer.

4.2.3 Multiscale Fusion Autoencoder

Multiscale Fusion Encoder. The encoder is responsible for gradually downsampling the input image and extracting high-level semantic features. To be able to make full use of the information of the images of the multiscale MS encoder and multiscale PAN encoder, it is necessary to deeply fuse \mathbf{S} and \mathbf{P} at the same scale. After multiscale MS and PAN encoders, we have two feature sets \mathbf{S} and \mathbf{P} , representing PAN and MS images, respectively. Since high-resolution MS images must have high spatial and spectral resolutions, their features must have both spatial and spectral information. To do this, the two feature sets must be concatenated and added at the same scale.

That is, $\mathbf{F}_1=\mathbf{S}_3 + \mathbf{P}_1$, $\mathbf{F}_2=\mathbf{S}_2 + \mathbf{P}_2$, and $\mathbf{F}_3=\mathbf{S}_1 + \mathbf{P}_3$. Then the block same as the multiscale MS encoder is used to encode the concatenated feature maps into a more compact representation after each addition, and the end of the multiscale fusion encoder (Fig. 4 (c)) is the feature set $\mathbf{E} = \left\{ \mathbf{E}_i \in \mathbb{R}^{(C \times 2^{i-1}) \times \frac{H}{2^{(i-1)}} \times \frac{W}{2^{(i-1)}}} \mid i \in [1, 2, 3] \right\}$, which encodes the spatial and spectral information of the two input images,

$$\mathbf{E}_1 = \text{Block}(\mathbf{F}_i), \quad (2)$$

$$\mathbf{E}_i = \text{Block}(\mathbf{S}_{4-i} + \mathbf{P}_i + (\text{Downsample}(\mathbf{E}_{i-1}))). \quad (3)$$

Multiscale Fusion Decoder. The decoder (Fig. 4 (c)) corresponds to the encoder, and the upsampled feature map is fused with the feature map in the corresponding encoder by the feature fusion operation. This can help to recover the detail and texture information of the image.

Specifically, we upsample the features of the set \mathbf{E} and superimpose and fuse them with the features of the corresponding scale of \mathbf{E} . In encoder downsampling, some details and local information may be lost due to the loss of information or resolution degradation caused by downsampling.

Therefore, in the process of decoding \mathbf{E} , multiscale injection of \mathbf{S} and \mathbf{P} can obtain the details and local information from the encoder in the decoder, which can effectively connect and fuse the low-level and high-level features,

and finally output the fusion result \mathbf{F}_o .

5. Experiments

5.1. Implementation Details

Training Settings. The dataset is divided into training, validation, and test sets in a ratio of 8:1:1, which means the training set comprises 4,718 image pairs, and both the validation and test sets contain 590 image pairs each. The batch size is set to 16. We used the Adam [26] optimizer with a learning rate of 0.002. If there is no improvement in the performance of the validation set for ten consecutive

epochs, the learning rate is reduced to 10%. Cascaded layers in the multiscale feature fusion are set to 3, and the initial number of channels for the CMFNet is 32. We used the MSE as the object function. The training was performed on four NVIDIA GeForce RTX 3090 GPUs.

Evaluation Metrics. The evaluation of pansharpening algorithms for PAN and MS image fusion involves adapting widely used image quality assessment (IQA) metrics. These metrics include peak signal-to-noise ratio (PSNR), structural similarity index (SSIM) [41], spectral angle mapper (SAM) [47], relative dimensionless global error synthesis (ERGAS) [36], spatial correlation coefficient (SCC) [49], and mean-square error (MSE, $\times 10^{-4}$). These metrics measure fidelity, similarity, spectral and spatial distortion, and spatial correlation. By employing these metrics, the performance of pansharpening algorithms can be objectively evaluated and compared in real-world scenarios. This evaluation framework enables comprehensive analysis and comparison of different methods for pansharpening.

5.2. Comparison with State-of-the-Arts

To assess the performance of CMFNet in the task of pansharpening, we have selected eight representative state-of-the-art (SOTA) methods from 2016 to 2023 for comparative analysis. These methods include PNN [33], Pannet [45], MSDCNN [46], TFNet [29], FusionNet [9], GPPNN [44], SRPPNN [3], and PGCU [53]. We conducted comprehensive experiments on the PanBench to evaluate the performance of our model. Then we performed experiments on various classification scenarios to ensure the generalizability of our model across diverse real-world contexts.

Quantitative Comparison. The comparative results of the nine algorithms on the PanBench are presented in Tab. 2, with the best values highlighted in bold black. Our proposed method achieves the best overall performance compared to other state-of-the-art pansharpening methods, firmly establishing its superiority. Specifically, in terms of PSNR, our method outperforms the closest competitor, TFNet, by approximately 1.67. In addition to PSNR, notable improvements can also be observed in other metrics, indicating reduced spectral distortion and preserved spatial textures. We also counted the index values of CMFNet in each scenario (Tab. 4) and satellite (Tab. 3). It can be seen that the performance of each metric is optimal due to the simple structure of the water. The evaluation metrics vary from satellite to satellite, which is consistent with objective facts.

Qualitative Comparison. We also present qualitative comparisons of visualization results (as shown in Fig. 5) to demonstrate the effectiveness of our method on representative samples from across the datasets. The images in the

Table 2. Quantitative metrics for all the comparison methods on the PanBench.

Method	PSNR \uparrow	SSIM \uparrow	SAM \downarrow	ERGAS \downarrow	SCC \uparrow	MSE \downarrow
PNN [33]	28.9029	0.7887	0.0750	4.4998	0.8992	25.5223
PanNet [45]	30.1465	0.8497	0.0702	3.8053	0.9234	18.5474
MSDCNN [46]	29.2675	0.8237	0.0761	4.1677	0.9139	21.7871
TFNet [29]	32.7018	0.8931	0.0600	2.8816	0.9486	11.9169
FusionNet [9]	24.4378	0.7175	0.0880	7.5029	0.7913	70.0308
GPPNN [44]	28.8901	0.8211	0.0842	4.2720	0.9124	22.3945
SRPPNN [3]	31.3186	0.8647	0.0666	3.3526	0.9344	15.5632
PGCU [53]	29.9692	0.8244	0.0759	3.9113	0.9167	19.5983
CMFNet [Ours]	34.3852	0.9139	0.0579	2.7846	0.9494	9.0428

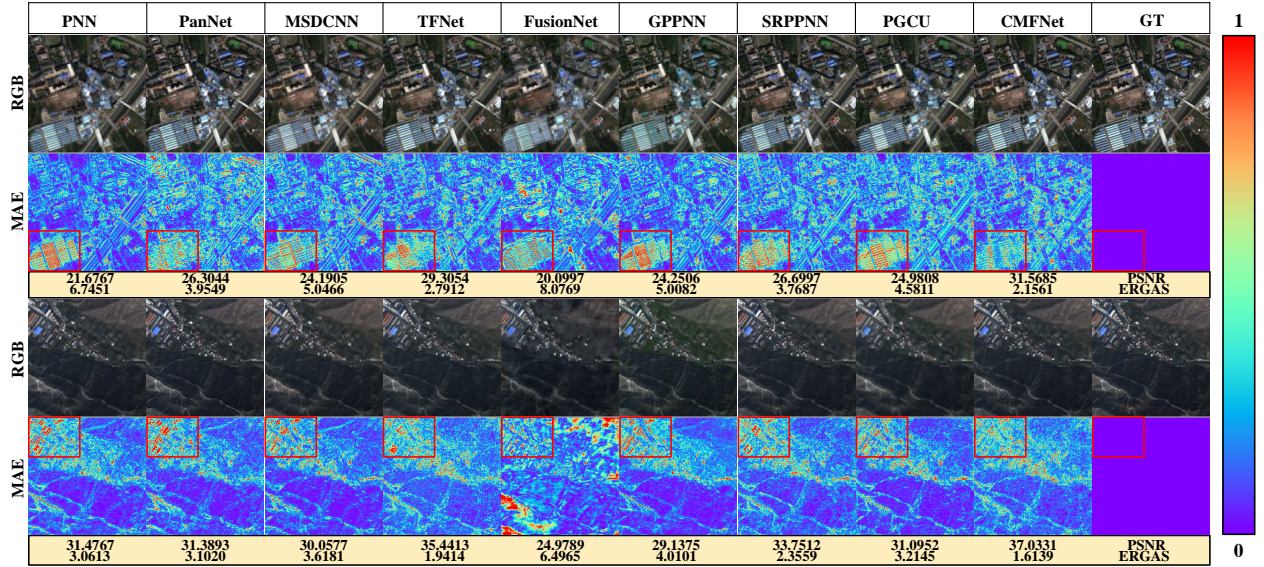


Figure 5. Visual results generated by different pansharpening methods. MAE denotes the mean absolute error across all spectral bands.

Table 3. Evaluation of CMFNet on each satellite of PanBench.

Satellite	PSNR \uparrow	SSIM \uparrow	SAM \downarrow	ERGAS \downarrow	SCC \uparrow	MSE \downarrow
GF1	42.8659	0.9591	0.0196	1.0457	0.9580	1.9661
GF2	36.6737	0.9554	0.0394	2.2247	0.9870	3.0906
GF6	34.2858	0.9165	0.0361	1.5311	0.9826	3.9269
LC7	36.6354	0.9391	0.0110	0.8417	0.9918	2.3282
LC8	30.0631	0.9055	0.0719	2.6224	0.9685	10.1524
WV2	34.8766	0.9424	0.0577	2.3661	0.9839	3.8216
WV3	35.2992	0.9350	0.0682	4.0791	0.8546	10.1377
WV4	29.7377	0.8751	0.0894	3.4016	0.9796	13.3450
QB	37.4593	0.9581	0.0506	1.4965	0.9897	2.0394
IN	25.1965	0.7549	0.0836	4.7192	0.8960	39.0390

second and fourth rows are the difference MAE between the output pansharpening results and the ground truth, where the red color means the generated effect is worse, and the

blue color means the generated effect is better. Our model has smaller spatial and spectral distortions compared to other competing methods. For MAE poor, we notice that our proposed method is closer to the ground truth than the other compared methods. This result proves the effectiveness of the proposed CMFNet, which successfully reduces information redundancy and enhances the quality of pansharpening results.

5.3. Ablation Studies

5.3.1 Impact of the Multiscale Cascading

By two decoupled MS and PAN encoders, we can obtain three hierarchical multiscale features with dimensions of 64×64 , 128×128 , and 256×256 . The autoencoder seamlessly fuses the corresponding features of the same scale in a cascading manner. As depicted in Tab. 5, we conducted experiments to investigate the impact of various cascading levels on the fusion outcomes. Notably, the performance of

Table 4. Evaluation of CMFNet on scene classification of PanBench.

Scene	PSNR \uparrow	SSIM \uparrow	SAM \downarrow	ERGAS \downarrow	SCC \uparrow	MSE \downarrow
Water	41.7804	0.9453	0.0363	2.1097	0.8990	4.3999
Urban	32.4035	0.9299	0.0632	2.8182	0.9807	8.5807
Ice/snow	34.0811	0.9290	0.0342	1.5132	0.9889	5.0679
Crops	35.7273	0.9449	0.0464	1.9383	0.9866	3.3005
Vegetation	32.4267	0.9045	0.0578	2.6551	0.9683	10.6414
Barren	32.9757	0.8848	0.0447	2.1215	0.9632	11.4405

Table 5. Impact of cascaded layers in the multiscale feature fusion.

Cascade	PSNR \uparrow	SSIM \uparrow	SAM \downarrow	ERGAS \downarrow	SCC \uparrow	MSE \downarrow
1	33.0352	0.8937	0.0579	2.7846	0.9494	10.9749
2	34.3852	0.9139	0.0516	2.4266	0.9595	9.0428
3	34.4921	0.9153	0.0511	2.3984	0.9601	8.8862

Table 6. Ablation study results on cascaded information injection.

Injection	PSNR \uparrow	SSIM \uparrow	SAM \downarrow	ERGAS \downarrow	SCC \uparrow	MSE \downarrow
\times	34.0757	0.9102	0.0528	2.4926	0.9568	9.5769
\checkmark	34.4921	0.9153	0.0511	2.3984	0.9601	8.8862

Table 7. Ablation study results on the scalability of PanBench dataset. Here, ‘‘SR’’, ‘‘CZ’’, and ‘‘PS’’ represent image super-resolution, image colorization, and pansharpening, respectively.

Task	PSNR \uparrow	SSIM \uparrow	SAM \downarrow	ERGAS \downarrow	SCC \uparrow	MSE \downarrow
SR (w/o PAN)	29.6283	0.7656	0.3256	25.9604	0.8205	25.3851
CO (w/o MS)	25.1988	0.7811	0.1686	7.9895	0.7782	50.1688
PS (MS+PAN)	34.3852	0.9139	0.0579	2.7846	0.9494	9.0428

pansharpening exhibits linear growth as the number of cascading layers increases, reaching its optimal state when the number of cascading layers equals three. This compellingly validates the necessity of hierarchically cascading fusion.

5.3.2 Impact of the Cascaded Injection

In the multiscale fusion decoder, we incorporate a cascading strategy for information injection, whereby the spectral information from the MS image and the spatial information from the PAN image are directly injected across the encoder into the decoder. To validate the effectiveness of this strategy, we conducted ablative research, and the experimental results are shown in Tab. 6. Following the introduction of cascading information injection, the PSNR increased by 0.4164, and the ERGAS decreased by approximately 0.1. The consistent performance improvements on

all metrics provide substantial evidence for the effectiveness of this strategy. One possible explanation is that for the computer vision task of pansharpening, which belongs to low-level visual computations, the cross-connection of feature injection serves as an efficacious means to alleviate the loss of information during the encoding process.

5.3.3 Scalability of the PanBench Dataset

It is worth mentioning that the PanBench dataset we constructed is not only suitable for pansharpening tasks in the field of remote sensing, but also supports other general computer vision tasks such as image super-resolution [16, 20, 38], image colorization [37], and image classification. In addition, we evaluated the performance of CMFNet on image super-resolution and image colorization tasks through ablation experiments, as shown in Tab. 7. Compared to pansharpening, super-resolution [52] reconstruction only receives PAN images as input, while colorization only receives MS images as input. As can be seen from Tab. 7, colorization is the most challenging task, followed by super-resolution and then pansharpening.

6. Conclusion

This paper presents PanBench, a large-scale, high-resolution, and multi-scene dataset encompassing the prominent satellites commonly used for pansharpening. The dataset is made available in an open-source manner, to facilitate the development of novel pansharpening methods. To achieve high-fidelity synthesis, we propose CMFNet, a new model designed explicitly for panchromatic sharpening. Experimental results on visual restoration and semantic recovery quality demonstrate the effectiveness of the proposed approach, surpassing existing representative pansharpening methods. The experimental findings also indicate the algorithm’s strong generalization capability and impressive performance. We firmly believe that the PanBench dataset will benefit the community, while our evaluations provide valuable directions for future research endeavors.

References

- [1] Anju Asokan and JJESI Anitha. Change detection techniques for remote sensing applications: A survey. *Earth Science Informatics*, 12:143–160, 2019. 1
- [2] Riccardo Barzaghi, Daniela Carrion, Marianna Carroccio, Renzo Maseroli, Giacomo Stefanelli, and Giovanna Venuti. Gravity corrections for the updated italian levelling network. *Applied Geomatics*, 15(3):773–780, 2023. 4
- [3] Jiajun Cai and Bo Huang. Super-resolution-guided progressive pansharpening based on a deep convolutional neural network. *IEEE Transactions on Geoscience and Remote Sensing*, 59(6):5206–5220, 2020. 2, 3, 6, 7
- [4] Xiangyong Cao, Jing Yao, Zongben Xu, and Deyu Meng. Hyperspectral image classification with convolutional neural network and active learning. *IEEE Transactions on Geoscience and Remote Sensing*, 58(7):4604–4616, 2020. 1
- [5] Xiangyong Cao, Xueyang Fu, Chen Xu, and Deyu Meng. Deep spatial-spectral global reasoning network for hyperspectral image denoising. *IEEE Transactions on Geoscience and Remote Sensing*, 60:1–14, 2021. 1
- [6] Liangyu Chen, Xiaojie Chu, Xiangyu Zhang, and Jian Sun. Simple baselines for image restoration. In *European Conference on Computer Vision*, pages 17–33, 2022. 5
- [7] Gong Cheng, Junwei Han, and Xiaoqiang Lu. Remote sensing image scene classification: Benchmark and state of the art. *Proceedings of the IEEE*, 105(10):1865–1883, 2017. 3, 4
- [8] Ilke Demir, Krzysztof Koperski, David Lindenbaum, Guan Pang, Jing Huang, Saikat Basu, Forest Hughes, Devis Tuia, and Ramesh Raskar. DeepGlobe 2018: A challenge to parse the earth through satellite images. In *IEEE Conference on Computer Vision and Pattern Recognition Workshop*, pages 172–181, 2018. 3, 4
- [9] Liang-Jian Deng, Gemine Vivone, Cheng Jin, and Jocelyn Chanussot. Detail injection-based deep convolutional neural networks for pansharpening. *IEEE Transactions on Geoscience and Remote Sensing*, 59(8):6995–7010, 2020. 1, 2, 3, 6, 7
- [10] Chao Dong, Chen Change Loy, Kaiming He, and Xiaoou Tang. Image super-resolution using deep convolutional networks. *IEEE Transactions on Pattern Analysis and Machine Intelligence*, 38(2):295–307, 2015. 1
- [11] Anaïs Gastineau, Jean-François Aujol, Yannick Berthoumieu, and Christian Germain. Generative adversarial network for pansharpening with spectral and spatial discriminators. *IEEE Transactions on Geoscience and Remote Sensing*, 60:1–11, 2021. 2
- [12] Ross Girshick. Fast r-cnn. In *IEEE International Conference on Computer Vision*, pages 1440–1448, 2015. 1
- [13] Kaiming He, Xiangyu Zhang, Shaoqing Ren, and Jian Sun. Deep residual learning for image recognition. In *IEEE Conference on Computer Vision and Pattern Recognition*, pages 770–778, 2016. 3
- [14] Kaiming He, Xiangyu Zhang, Shaoqing Ren, and Jian Sun. Deep residual learning for image recognition. In *IEEE Conference on Computer Vision and Pattern Recognition*, pages 770–778, 2016. 5
- [15] Xiaolin Hu, Kai Li, Weiyi Zhang, Yi Luo, Jean-Marie Lemerrier, and Timo Gerkmann. Speech separation using an asynchronous fully recurrent convolutional neural network. *Advances in Neural Information Processing Systems*, 34:22509–22522, 2021. 1
- [16] Jianqiang Huang, Kai Li, and Xiaoying Wang. Single image super-resolution reconstruction of enhanced loss function with multi-gpu training. In *ISPA/BDCloud/SocialCom/Su*, pages 559–565, 2019. 8
- [17] Wei Huang, Liang Xiao, Zhihui Wei, Hongyi Liu, and Songze Tang. A new pan-sharpening method with deep neural networks. *IEEE Geoscience and Remote Sensing Letters*, 12(5):1037–1041, 2015. 3
- [18] Kui Jiang, Zhongyuan Wang, Peng Yi, Junjun Jiang, Jing Xiao, and Yuan Yao. Deep distillation recursive network for remote sensing imagery super-resolution. *Remote Sensing*, 10(11):1700, 2018. 1
- [19] Xin Jin, Shanshan Huang, Qian Jiang, Shin-Jye Lee, Liwen Wu, and Shaowen Yao. Semisupervised remote sensing image fusion using multiscale conditional generative adversarial network with siamese structure. *IEEE Journal of Selected Topics in Applied Earth Observations and Remote Sensing*, 14:7066–7084, 2021. 3
- [20] Kai Li, Shenghao Yang, Runting Dong, Xiaoying Wang, and Jianqiang Huang. Survey of single image super-resolution reconstruction. *IET Image Processing*, 14(11):2273–2290, 2020. 8
- [21] Kai Li, Runxuan Yang, and Xiaolin Hu. An efficient encoder-decoder architecture with top-down attention for speech separation. *International Conference on Learning Representations*, pages 1–13, 2022. 1
- [22] Xiao Li, Ziqi Wang, Bo Zhang, Fuchun Sun, and Xiaolin Hu. Recognizing object by components with human prior knowledge enhances adversarial robustness of deep neural networks. *IEEE Transactions on Pattern Analysis and Machine Intelligence*, 2023. 1
- [23] Shunlin Liang, Hongliang Fang, and Mingzhen Chen. Atmospheric correction of landsat etm+ land surface imagery. i. methods. *IEEE Transactions on Geoscience and Remote Sensing*, 39(11):2490–2498, 2001. 4
- [24] Stephen Lin, Jinwei Gu, Shuntaro Yamazaki, and Heung-Yeung Shum. Radiometric calibration from a single image. In *IEEE Conference on Computer Vision and Pattern Recognition*, pages II–II, 2004. 4
- [25] Junmin Liu, Shijie Li, Changsheng Zhou, Xiangyong Cao, Yong Gao, and Bo Wang. SRAF-Net: A scene-relevant anchor-free object detection network in remote sensing images. *IEEE Transactions on Geoscience and Remote Sensing*, 60:1–14, 2021. 1
- [26] Mingrui Liu, Wei Zhang, Francesco Orabona, and Tianbao Yang. Adam: A stochastic method with adaptive variance reduction. pages 1–23, 2021. 6
- [27] Qingjie Liu, Huanyu Zhou, Qizhi Xu, Xiangyu Liu, and Yunhong Wang. PSGAN: A generative adversarial network for remote sensing image pan-sharpening. *IEEE Transactions on Geoscience and Remote Sensing*, 59(12):10227–10242, 2020. 2, 3

- [28] Qiang Liu, Xiangchao Meng, Feng Shao, and Shutao Li. Supervised-unsupervised combined deep convolutional neural networks for high-fidelity pansharpening. *Information Fusion*, 89:292–304, 2023. 2, 3
- [29] Xiangyu Liu, Qingjie Liu, and Yunhong Wang. Remote sensing image fusion based on two-stream fusion network. *Information Fusion*, 55:1–15, 2020. 1, 2, 6, 7
- [30] Zhuang Liu, Hanzi Mao, Chao-Yuan Wu, Christoph Feichtenhofer, Trevor Darrell, and Saining Xie. A convnet for the 2020s. In *IEEE Conference on Computer Vision and Pattern Recognition*, pages 11976–11986, 2022. 5
- [31] ZhiYong Lv, PengFei Zhang, WeiWei Sun, Jón Atli Benediktsson, JunHuai Li, and Wei Wang. Novel adaptive region spectral-spatial features for land cover classification with high spatial resolution remotely sensed imagery. *IEEE Transactions on Geoscience and Remote Sensing*, 2023. 1
- [32] Jiayi Ma, Wei Yu, Chen Chen, Pengwei Liang, Xiaojie Guo, and Junjun Jiang. Pan-GAN: An unsupervised pansharpening method for remote sensing image fusion. *Information Fusion*, 62:110–120, 2020. 1
- [33] Giuseppe Masi, Davide Cozzolino, Luisa Verdoliva, and Giuseppe Scarpa. Pansharpening by convolutional neural networks. *Remote Sensing*, 8(7):594, 2016. 1, 2, 6, 7
- [34] Qingyan Meng, Maofan Zhao, Linlin Zhang, Wenxu Shi, Chen Su, and Lorenzo Bruzzone. Multilayer feature fusion network with spatial attention and gated mechanism for remote sensing scene classification. *IEEE Geoscience and Remote Sensing Letters*, 19:1–5, 2022. 4
- [35] Qingyan Meng, Wenxu Shi, Sijia Li, and Linlin Zhang. Pan-Diff: A novel pansharpening method based on denoising diffusion probabilistic model. *IEEE Transactions on Geoscience and Remote Sensing*, 2023. 2, 3
- [36] Diego Renza, Estibaliz Martinez, and Agueda Arquero. A new approach to change detection in multispectral images by means of ergas index. *IEEE Geoscience and Remote Sensing Letters*, 10(1):76–80, 2012. 6
- [37] Chitwan Saharia, William Chan, Huiwen Chang, Chris Lee, Jonathan Ho, Tim Salimans, David Fleet, and Mohammad Norouzi. Palette: Image-to-image diffusion models. In *ACM SIGGRAPH*, pages 1–10, 2022. 8
- [38] Chitwan Saharia, Jonathan Ho, William Chan, Tim Salimans, David J Fleet, and Mohammad Norouzi. Image super-resolution via iterative refinement. *IEEE Transactions on Pattern Analysis and Machine Intelligence*, 45(4):4713–4726, 2022. 8
- [39] Zhimin Shao, Zexin Lu, Maosong Ran, Leyuan Fang, Jiliu Zhou, and Yi Zhang. Residual encoder–decoder conditional generative adversarial network for pansharpening. *IEEE Geoscience and Remote Sensing Letters*, 17(9):1573–1577, 2019. 1
- [40] Lucien Wald, Thierry Ranchin, and Marc Mangolini. Fusion of satellite images of different spatial resolutions: Assessing the quality of resulting images. *Photogrammetric Engineering and Remote Sensing*, 63(6):691–699, 1997. 3
- [41] Zhou Wang, A.C. Bovik, H.R. Sheikh, and E.P. Simoncelli. Image quality assessment: from error visibility to structural similarity. *IEEE Transactions on Image Processing*, 13(4):600–612, 2004. 6
- [42] Zhongyuan Wang, Kui Jiang, Peng Yi, Zhen Han, and Zheng He. Ultra-dense gan for satellite imagery super-resolution. *Neurocomputing*, 398:328–337, 2020. 1
- [43] Chen Wu, Bo Du, and Liangpei Zhang. Fully convolutional change detection framework with generative adversarial network for unsupervised, weakly supervised and regional supervised change detection. *IEEE Transactions on Pattern Analysis and Machine Intelligence*, 2023. 1
- [44] Shuang Xu, Jianshe Zhang, Zixiang Zhao, Kai Sun, Junmin Liu, and Chunxia Zhang. Deep gradient projection networks for pan-sharpening. In *IEEE Conference on Computer Vision and Pattern Recognition*, pages 1366–1375, 2021. 1, 2, 3, 6, 7
- [45] Junfeng Yang, Xueyang Fu, Yuwen Hu, Yue Huang, Xinghao Ding, and John Paisley. PanNet: A deep network architecture for pan-sharpening. In *IEEE International Conference on Computer Vision*, pages 5449–5457, 2017. 1, 2, 3, 6, 7
- [46] Qiangqiang Yuan, Yancong Wei, Xiangchao Meng, Huanfeng Shen, and Liangpei Zhang. A multiscale and multidepth convolutional neural network for remote sensing imagery pan-sharpening. *IEEE Journal of Selected Topics in Applied Earth Observations and Remote Sensing*, 11(3):978–989, 2018. 1, 2, 6, 7
- [47] Roberta H Yuhas, Alexander FH Goetz, and Joe W Boardman. Discrimination among semi-arid landscape endmembers using the spectral angle mapper (sam) algorithm. In *JPL Airborne Geoscience Workshop*, pages 147–149, 1992. 6
- [48] Hao Zhang and Jiayi Ma. GTP-PNet: A residual learning network based on gradient transformation prior for pansharpening. *ISPRS Journal of Photogrammetry and Remote Sensing*, 172:223–239, 2021. 1
- [49] Jie Zhou, Daniel L Civco, and John A Silander. A wavelet transform method to merge landsat tm and spot panchromatic data. *International Journal of Remote Sensing*, 19(4):743–757, 1998. 6
- [50] Man Zhou, Jie Huang, Keyu Yan, Hu Yu, Xueyang Fu, Aiping Liu, Xian Wei, and Feng Zhao. Spatial-frequency domain information integration for pan-sharpening. In *European Conference on Computer Vision*, pages 274–291, 2022. 1, 2, 3
- [51] Man Zhou, Keyu Yan, Jie Huang, Zihe Yang, Xueyang Fu, and Feng Zhao. Mutual information-driven pan-sharpening. In *IEEE Conference on Computer Vision and Pattern Recognition*, pages 1798–1808, 2022. 1, 2, 3
- [52] Man Zhou, Keyu Yan, Jinshan Pan, Wenqi Ren, Qi Xie, and Xiangyong Cao. Memory-augmented deep unfolding network for guided image super-resolution. *International Journal of Computer Vision*, 131(1):215–242, 2023. 8
- [53] Zeyu Zhu, Xiangyong Cao, Man Zhou, Junhao Huang, and Deyu Meng. Probability-based global cross-modal upsampling for pansharpening. pages 14039–14048, 2023. 2, 3, 6, 7
- [54] Xuechao Zou, Kai Li, Junliang Xing, Yu Zhang, Shiyang Wang, Lei Jin, and Pin Tao. DiffCR: A fast conditional diffusion framework for cloud removal from optical satellite images, 2023. 5